Electrochimica Acta 55 (2009) 218–226

Contents lists available at ScienceDirect

Electrochimica Acta

journal homepage: www.elsevier.com/locate/electacta

In situ STM studies of Ga electrodeposition from $GaCl_3$ in the air- and water-stable ionic liquid 1-butyl-1-methylpyrrolidinium bis(trifluoromethylsulfonyl)amide

L.H.S. Gasparotto[a,b,c], N. Borisenko[a,b], O. Höfft[a], R. Al-Salman[a], W. Maus-Friedrichs[d,e], N. Bocchi[c], S. Zein El Abedin[a,b], F. Endres[a,b,*]

[a] *Institut für Mechanische Verfahrenstechnik, Clausthal University of Technology, Arnold-Sommerfeld-Straße 6, D-38678 Clausthal-Zellerfeld, Germany*
[b] *EFZN Goslar, Am Stollen 19, D-38640 Goslar, Germany*
[c] *Universidade Federal de São Carlos, DQ, CP 676, São Carlos, SP 13565-905, Brazil*
[d] *Institut für Physik und Physikalische Technologien, Clausthal University of Technology, Leibnizstr. 4, D-38678 Clausthal-Zellerfeld, Germany*
[e] *Clausthaler Zentrum für Materialtechnik, Clausthal University of Technology, D-38678 Clausthal-Zellerfeld, Germany*

ARTICLE INFO

Article history:
Received 8 July 2009
Received in revised form 20 August 2009
Accepted 21 August 2009
Available online 31 August 2009

Keywords:
Electrodeposition
Ionic liquid
Gallium
In situ STM
Solvation layer

ABSTRACT

In the present paper the electrodeposition of Ga on Au(1 1 1) from 0.5 mol L^{-1} $GaCl_3$ in the air- and water-stable ionic liquid 1-butyl-1-methylpyrrolidinium bis(trifluoromethylsulfonyl)amide, $[Py_{1,4}]$TFSA, has been investigated by *in situ* scanning tunneling microscopy (STM), X-ray photoelectron spectroscopy (XPS), scanning electron microscopy (SEM) and cyclic voltammetry (CV). The CV shows two redox processes: the one at −0.3 V *vs.* Pt is attributed to a Ga deposition on a Ga layer formed during an electroless deposition process at OCP and/or to the formation of a Au–Ga alloy; the other one at −0.9 V is due to the bulk deposition of Ga. The XPS measurement reveals that there is an oxide layer on the top of the gallium electrodeposit due to exposure to air. *In situ* STM measurements show that the first layer of the Ga deposit consists of islands of 10–30 nm in width and several nanometers in height surprisingly the result of an electroless deposition at the OCP. If the electrode potential is further reduced the bulk deposition of Ga sets in.

1. Introduction

Gallium is a soft silvery-metallic element vastly applied in optoelectronics (e.g., LED's), non-linear and quantum optics, production of III–V semiconductors and many commercial items such as alloys, computers and DVD's. The electrodeposition of Ga has been applied for its extraction and purification [1] and production of III–V semiconductors [2]. As gallium is largely used for the fabrication of semiconductors, a fine control of its deposit structure is required. Electrodeposition is useful for the preparation of new materials with specific features (thin layers, dispersed materials and nanostructures), especially of the transition elements and of semiconductor compounds. Gallium is usually extracted as a by-product in the aluminium (from Bayer-process liquors) and zinc industries [3]. However the electrodeposition of Ga from aqueous media is often complicated by hydrogen evolution especially in acidic solutions, resulting in poor current efficiencies and non-uniform deposits [4,5]. Recently Flamini et al. [6,7] reported the electrodeposition of gallium on vitreous carbon, aluminium and aluminium-zinc electrodes from a Ga(III)-chloride aqueous solution. At low potentials Ga(III) is reduced to Ga(I) on vitreous carbon while at more negative potentials gallium deposition occurs simultaneously with the hydrogen evolution. The presence of zinc facilitates Ga enrichment at the interface and improves the wetting on the aluminium oxide leading to the formation of a Ga–Al alloy at the surface. Hydrogen evolution is the main parasitic process that impedes the use of aqueous solvents for the electrodeposition of Ga. To date no method has been published describing the electrodeposition of Ga from organic solvents.

The alternative to molecular solvents is to use ionic liquids especially those that are liquid below 100 °C. Room temperature ionic liquids (RTILs) have attracted immense interest in the recent few years. The advantages of RTILs include good chemical and thermal stability, almost negligible vapour pressure, good electrical conductivity and a wide electrochemical window (up to 6 V), allowing the deposition of materials which cannot be obtained in aqueous solutions [8–10]. Today about 300 various ionic liquids with different properties and qualities are commercially available.

In 1986 Wicelinski and Gale [11] showed that Ga–As can, in principle, be electrodeposited from $GaCl_3$ and $AsCl_3$ at 40 °C in

* Corresponding author at: Institut für Mechanische Verfahrenstechnik, Clausthal University of Technology, Arnold-Sommerfeld-Straße 6, D-38678 Clausthal-Zellerfeld, Germany. Tel.: +49 5323 72 3141; fax: +49 5323 72 2460.
E-mail address: frank.endres@tu-clausthal.de (F. Endres).

0013-4686/$ – see front matter © 2009 Elsevier Ltd. All rights reserved.
doi:10.1016/j.electacta.2009.08.041

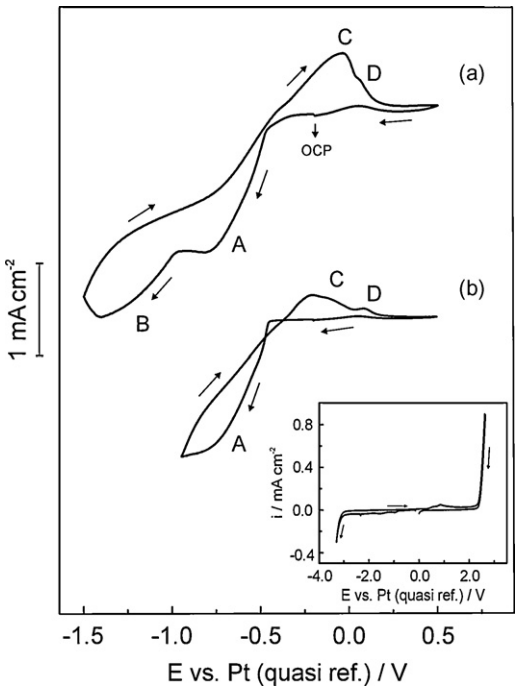

Fig. 1. Cyclic voltammograms of 0.5 mol L^{-1} $GaCl_3$ in $[Py_{1,4}]$TFSA on Au(1 1 1) at 25 °C: (a) limit negative potential of −1.5 V *vs.* Pt. (b) Limit negative potential of −0.9 V *vs.* Pt. *Inset*: the cyclic voltammogram of the ultrapure dry $[Py_{1,4}]$TFSA on Au(1 1 1) at 25 °C. The electrochemical window is of about 5.5 V limited by the irreversible reduction of the organic cation and gold oxidation. Scan rates are 10 mV s^{-1}.

the Lewis acid chloroaluminate ionic liquid composed of $AlCl_3$ and 1-butylpyridinium chloride. The authors reported that Al codeposition occurs in the underpotential deposition regime on the Ga surface. In order to exclude Al contamination Carpenter and Verbrugge [12,13] employed a chlorogallate ionic liquid. It was shown that Ga–As film can be obtained at room temperature in the Lewis basic $GaCl_3$/1-ethyl-3-methylimidazolium chloride ionic liquid, to which $AsCl_3$ was added. In our experience chlorogallate ionic liquids are chemically extremely aggressive.

In 1999 Sun et al. [14] reported that gallium can be electrodeposited from Lewis acid aluminium chloride/1-ethy-3-methylimidazolium chloride, $AlCl_3$/[EMIM]Cl (ratio 60/40 mol%) ionic liquid on glassy carbon and on tungsten rotating disk electrodes. Elemental gallium was electrodissolved in the ionic liquid producing a Ga(I) solution which can be electrochemically oxidized to Ga(III). The gallium films obtained on tungsten at 30 °C were liquid uniformly covering the electrode surface. If glassy carbon is applied as a working electrode the authors reported a three-dimensional nucleation of gallium with diffusion-controlled growth of nuclei. It was shown that Ga reacts with Ga(III) forming Ga(I). In 2003 Smolenskii et al. briefly reported that gallium can be electrodeposited on tungsten from its trichloride in 1-ethyl-3-methylimidazolium bis(trifluoromethylsulfonyl)amide, [EMIM]TFSA. However, no details of the electrochemical process neither images of the deposit were presented [15].

In the present study we employed the room temperature air- and water-stable ionic liquid 1-butyl-1-methylpyrrolidinium bis(trifluoromethylsulfonyl)amide, $[Py_{1,4}]$TFSA—due to its wide electrochemical window—for Ga electrodeposition. We present for the first time an *in situ* scanning tunneling microscopy (STM) study of gallium electrodeposition from $GaCl_3$ (0.5 M) on Au(1 1 1). Scanning electron microscopy (SEM), energy-dispersive X-ray spectroscopy (EDX) and X-ray photoelectron spectroscopy (XPS) were used for *ex situ* characterization of the electrodeposits.

2. Experimental

1-Butyl-1-methylpyrrolidinium bis(trifluoromethylsulfonyl)-amide, $[Py_{1,4}]$TFSA, ionic liquid was purchased from IOLITEC in the highest available quality (chloride <10 ppm, alkali free synthesis). This ionic liquid has a wide electrochemical window of about 5 V on Au(1 1 1) [16] and a not too high viscosity of 85 mPa s at 25 °C [17]. Before use the liquid was dried under vacuum at 120 °C to a water content well below 1 ppm and stored in a closed bottle in an argon-filled glove box with water and oxygen contents below 2 ppm (OMNI-LAB from Vacuum-Atmospheres). $GaCl_3$ (99.999%) was purchased from Aldrich Co. The working electrode was Au(1 1 1) (a 300 nm thick film on mica) purchased from Agilent Technologies. Prior to use the substrates were carefully heated in a hydrogen flame to minimize possible surface contaminations. A Pt-wire and a Pt-ring were also heated in the hydrogen flame to remove organic contaminations and used as quasi-reference and counter electrodes, respectively. All potentials are referred to the Pt quasi reference electrode. We are well aware that Pt quasi-reference electrodes are not optimal, but currently still the only choice for *in situ* STM experiments if any contamination shall be excluded. This electrode shows usually a sufficiently good stability, especially during the STM experiments. The electrochemical cell was made of Teflon and clamped over a Teflon covered Viton o-ring onto the substrate, thus yielding a geometric surface area of the working electrode of 0.3 cm^2. All parts of the electrochemical cell in contact with the electrolyte were cleaned in a mixture of 50/50 vol.% H_2SO_4/H_2O_2 followed by refluxing in pyrogene free water (aqua destillata ad iniectabilia) prior to use. The electrochemical measurements were carried out using a PARSTAT 2263 potentiostat/galvanostat controlled by a PowerSuite software. For scanning electron microscopy (SEM) and energy-dispersive X-ray spectroscopy (EDX) the working electrode with the deposit on it was removed from the glove box, washed with isopropanol in order to remove traces of the ionic liquid, dried under vacuum and stored in the glove box before analysis. SEM and EDX analyses were carried out in a high-resolution field emission scanning electron microscope (Carl Zeiss DSM 982 Gemini). The used EDX system has a maximum chemical sensitivity of 0.05 wt.%. The chemical composition of the film surface was analysed *ex situ* with X-ray photoelectron spectroscopy (XPS). XPS was performed using a commercial non-monochromatic X-ray source (Fisons XR3E2-324). The spectra were recorded under UHV conditions (10^{-10} mbar) using Al K_α

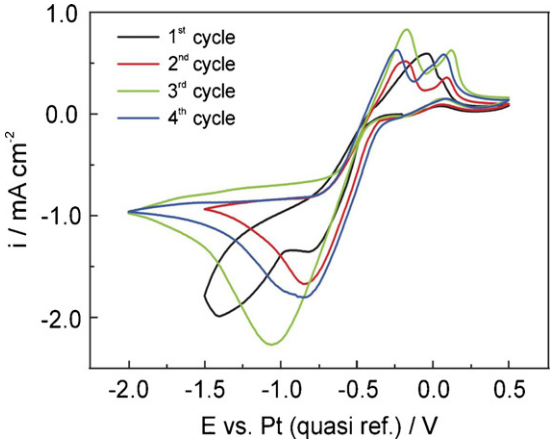

Fig. 2. Cyclic voltammograms of 0.5 mol L^{-1} $GaCl_3$ in $[Py_{1,4}]$TFSA on Au(1 1 1) at 25 °C. In the 1st scan two reduction processes are obtained. The first peak disappears in the subsequent scans once the gold surface is no longer available and the deposition takes place on an altered surface. Scan rates are 10 mV s^{-1}.

primary radiation (14 kV, 20 mA, 1486.6 eV). After acquisition of the spectra, various data handling procedures were carried out on the raw data. Survey (broad energy range, low resolution) spectra were collected to determine the elemental composition of the sample surfaces. Spectra with better resolution than 1.5 eV (Ag $3d_{5/2}$ at 40 eV pass energy) of the Ga 2p core levels were collected to determine chemical/bonding states. All given values in eV are referenced to the C1s peak (in this case C1s = 285 eV). XPS provides information on the outermost 5–10 nm of the sample. XPS peaks were fitted mathematically using overlapping Gauss profiles. The fitting was performed applying OriginPro7 including the Peak Fitting Module (OriginLab Corporation). The *in situ* scanning tunneling microscopy (STM) experiments were performed with in house designed STM heads and scanners under inert gas conditions with a Molecular Imaging PicoScan 2500 STM controller in feedback mode. Assembling of the STM head and filling of the electrochemical cell were performed in a second glove box solely reserved for assembling of STM heads. The STM head was placed inside an argon-filled stainless steel cylinder, thus ensuring inert gas during the STM experiment, transferred to the air-conditioned laboratory with a constant temperature of 23 ± 1 °C and placed onto a vibration damped table from IDE (Germany). STM tips were prepared by electrochemical etching of 0.25 mm 90/10 Pt/Ir wires in 4 M NaCN solution followed by electrophoretical coating with an electropaint from BASF (ZQ 84-3225 0201). During the STM experiments the potential of the working electrode was controlled by the PicoStat from Molecular Imaging. In all experiments the STM images were obtained by scanning from the bottom to the top of a picture with a scan rate of 2 Hz and a resolution of 512 pixels per line. For the current–voltage tunneling spectroscopy the tip was positioned on the site of interest and the tip voltage was varied between an upper and a lower limit. During this measurement the feedback is automatically switched off by the software. For the electroless deposition experiments, gold substrates (an about 300 nm layer of Au deposited on glass, purchased from Arrandee) were carefully heated in a hydrogen flame to minimize possible surface contaminations and immediately placed in the glove box. The substrates were immersed in a 0.5 mol L^{-1} $GaCl_3$/$[Py_{1,4}]$TFSA solution for 1 h at 24 °C, 36 °C and 60 °C. For the SEM examination, the samples were removed and rinsed gently with isopropanol to wash off the ionic liquid residues.

3. Results and discussion

3.1. Cyclic voltammetry

The electrochemical behavior of 0.5 mol L^{-1} $GaCl_3$ in the ionic liquid $[Py_{1,4}]$TFSA on Au(1 1 1) at room temperature is presented in Fig. 1. Scans were swept cathodically from the initial potential −0.2 V *vs.* Pt at a scan rate of 10 mV s^{-1}. The electrochemical window of the employed dry ionic liquid $[Py_{1,4}]$TFSA on Au(1 1 1) is a little more than 5 V as can be seen in the cyclic voltammogram (CV) of the inset in Fig. 1. At the cathodic limit the irreversible reduction of the organic cation is obtained at about −3.2 V *vs.* Pt-quasi ref. At the anodic limit gold dissolution occurs at +2.3 V.

Upon addition of 0.5 M $GaCl_3$, two reduction processes (*A* and *B*) and two anodic peaks (*C* and *D*) appear, as depicted in Fig. 1a. As will be shown by the *in situ* STM experiments below, a first monolayer of the deposit forms even if the potentiostat is switched off. The first cathodic process at −0.3 V (*A*) is attributed to the gallium

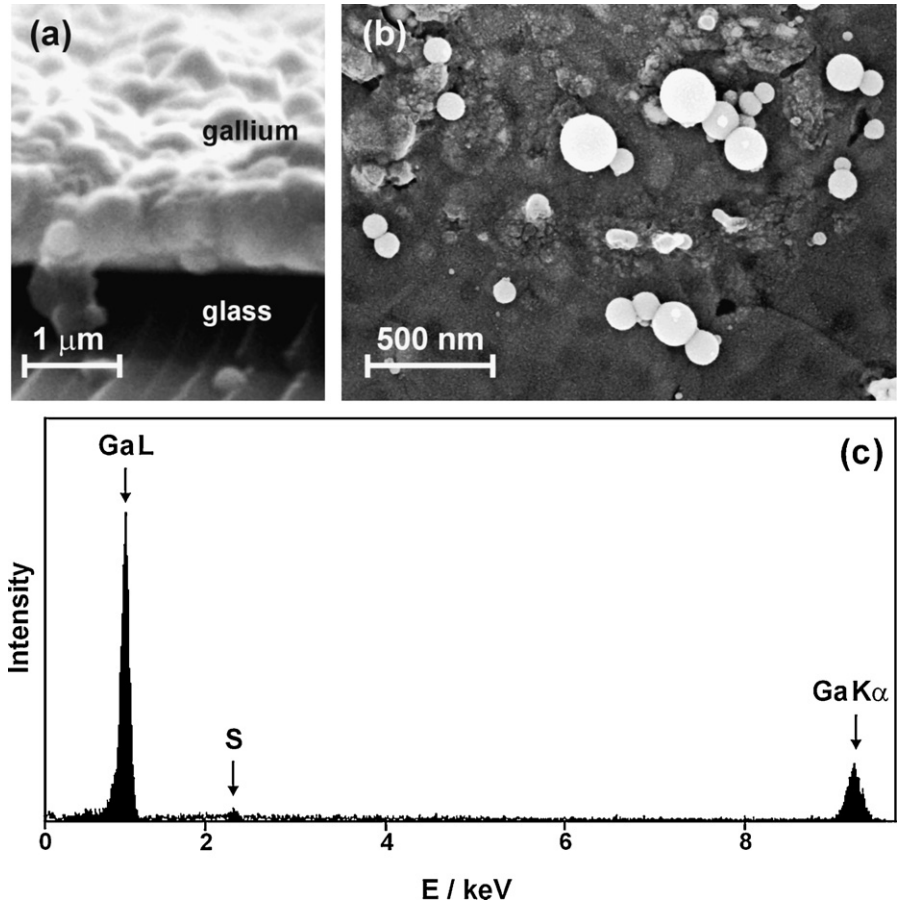

Fig. 3. SEM micrographs (secondary electrons) of gold surface with gallium electrodeposited potentiostatically at −1.5 V *vs.* Pt for 1 h: (a) side view, (b) top view and (c) EDX spectrum of the electrodeposit.

deposition on the gold surface, followed by further gallium deposition at *B* on the just-formed phase. The first process (*A*) is also correlated with the formation of a Au–Ga alloy, since its formation is reported to be energetically favored [18]. Yamanaka and Ino [19] reported that if more than one monolayer of Ga is deposited on $\sqrt{3} \times \sqrt{3}$ Au on Si(1 1 1), a Ga–Au alloy is formed. This explains the split of the Ga deposition in two peaks (*A* and *B*) as the surface is neither pure Au nor pure Ga. If highly oriented pyrolytic graphite (HOPG) substrate is used as a working electrode, only one cathodic and one anodic peaks are observed, which was expected as there is no alloying between gallium and carbon. The series of anodic processes (*C* and *D*) in the reverse scan is due to the partial dissolution of gallium from the bulk phase and the alloy, respectively. If the scan is reversed at −0.9 V (the potential regime of *A*) the voltammograms recorded exhibit a current loop indicative of a nucleation-controlled process (Fig. 1b). The two anodic processes (*C* and *D*) are also obtained, which is a further hint that a Ga–Au alloy is formed even at less negative electrode potentials. We would like to mention that the oxidation peaks *C* and *D* do not appear in the case of HOPG, which means that Ga reacts strongly with gold. Interestingly, the second cathodic peak *B* disappears in the subsequent cycles as can be seen in Fig. 2 probably due to a strong surface alteration by alloying of gold with gallium. Furthermore the potentials of the oxidation peaks shift with cycling as a result of the formation of bulk alloys at the surface during the cathodic scan. If the electrode potential is kept either at −1.5 V or at −0.9 V a grayish deposit is formed on the electrode surface.

3.2. Ex situ SEM and XPS studies

The morphology and the elemental composition of the deposit made potentiostatically at −1.5 V *vs*. Pt for 1 h were studied *ex situ* with high-resolution scanning electron microscopy (SEM) and energy-dispersive X-ray spectroscopy (EDX). The SEM micrograph in Fig. 3a presents a side view of the rough Ga deposit on Au (300 nm thick layer on glass substrate) with the average thickness of about 1 μm. As the thickness of the gold layer is only 300 nm, the Ga deposit itself is about 700 nm thick. Some spherical particles of 40–220 nm in diameter grow above the deposited layer (Fig. 3b). From this picture it is likely to conclude that the particles do not wet the surface (the contact angle is more than 90°). This is not typical for pure gallium on metal surfaces (Ga, Au or their alloy) and can be either attributed to the oxidation of the surface due to exposure to air or to solvation layers of the ionic liquid preventing a good wetting of gallium in the bulk phase. UHV experiments

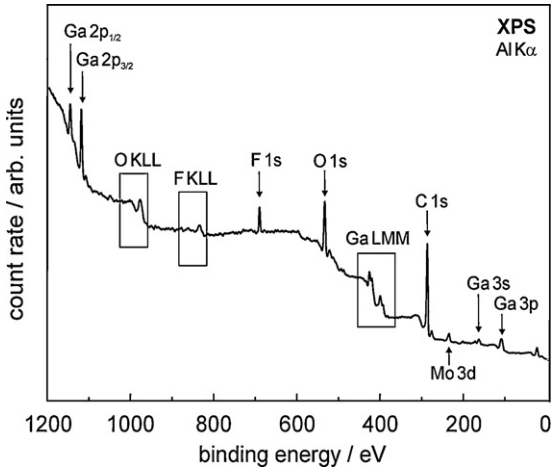

Fig. 4. XPS spectrum of a gallium film on HOPG substrate. The major spectral contributions are gallium, carbon, oxygen and fluorine.

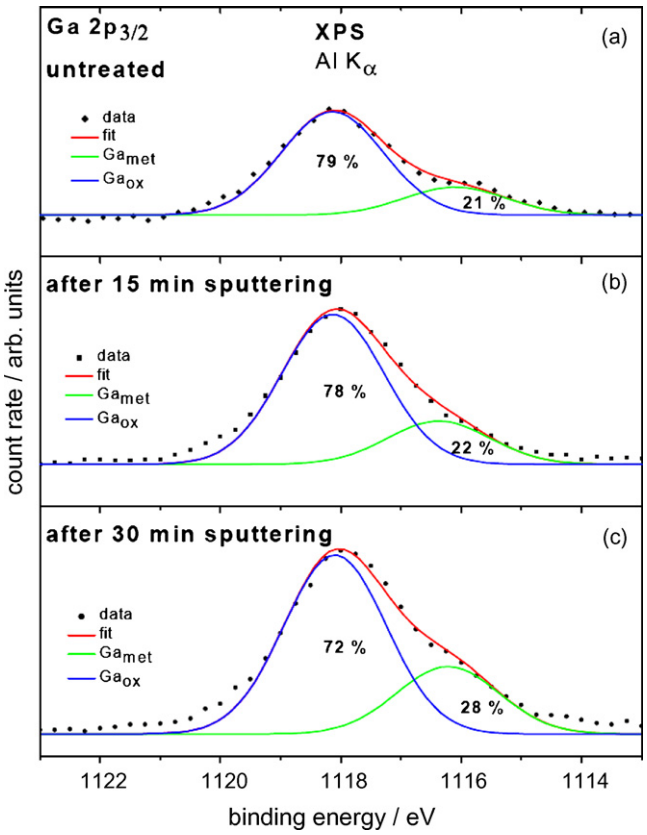

Fig. 5. High-resolution XPS spectrum of the Ga $2p_{3/2}$ core levels (a) neat. (b and c) Sputtered sample for 15 min each. *Dots*: original data obtained from the measurement. Peak fits of the individual components are displayed using coloured solid lines, while their sum is shown as the red solid line.

on the physical vapour deposition of Ag on pure and ionic liquid modified surfaces show that nucleation processes are influenced by ionic liquids. Quite recently we could show with partners [20] that ionic liquids form on Au(1 1 1) surprisingly strongly adhering solvation layers. Different ionic liquids form different solvation layers on solids like mica [21], graphite [22], leuco-sapphire [23] and Au(1 1 1) [20]. The adsorption is dependent on the ionic liquid and as an example $[Py_{1,4}]$TFSA is roughly four times more strongly adsorbed than [EMIm]TFSA. Up to seven adsorbed monolayers have been reported by different authors for different liquids. Theoretical considerations from Fedorov and Kornyshev [24] show that there is even no classical double layer in ionic liquids but rather multilayers as the experiments suggest. Ouchi and Katayama [25] reported on a poster on COIL-3 (3rd congress on ionic liquids) in Cairns, Australia, 2009, at the example of 1-butyl-1-methylimidazolium bis(trifluoromethylsulfonyl)amide on the potential dependence of solvation layers: in the cathodic regime there is a cation adsorption, in the anodic regime anion adsorption prevails and there is a strong hysteresis when moving back- and forward on the potential scale. These relatively new observations imply that solvation layers must influence electrochemical and in more general interface reactions in ionic liquids. The EDX analysis (Fig. 3c) gives Ga and some S from the residue of the electrolyte. No oxygen was observed, which means that this element is not a constituent of the bulk. EDX also shows that the spheres are composed solely of gallium. We cannot totally exclude that the spheres are a result of a melting process, as the melting point of pure gallium is close to 30 °C.

The chemical composition of the film surface was analysed *ex situ* with X-ray photoelectron spectroscopy (XPS). Fig. 4 represents the XPS survey spectrum of the gallium film on highly oriented pyrolytic graphite (HOPG). HOPG was used for this experiment in

order to avoid charging problems (the gold substrates are made of a thin gold layer on mica or glass, therefore charging effects would be inevitable). The major spectral contributions are gallium, carbon, oxygen and fluorine. The peak at around 230 eV is a contribution from the molybdenum sample holder. This does neither influence the results nor the interpretation. Carbon and fluorine are due to some residues from the ionic liquid. As the substrate area under investigation is larger than the deposit area, some of the carbon signal also results from the HOPG substrate. The energetic peak positions for the Ga $2p_{3/2}$ at about 1118 eV and for the Ga $2p_{1/2}$ at 1145 eV are in very good agreement with literature values given for Ga_2O_3 [26,27]. In order to remove most of the top-layer residues the deposited film was sputtered with Ar^+ ions two times (15 min each; E_{kin}: 4 keV, flux: 20 mA; angle of incidence 10°). The spectrum of the Ga $2p_{3/2}$ peak region obtained before and after the sputtering cycles is shown in Fig. 5 (a: neat, b and c sputtered sample). The dotted line represents the original data, peak fits of the individual components are displayed using coloured solid lines, while their sum is shown as the red solid line. In all spectra the Ga $2p_{3/2}$ peak is comprised of two contributions with binding energies at 1118 eV (blue line) and 1116 eV (green line). After the first sputtering cycle (Fig. 5b) the ratio between the two peaks was nearly the same. This is because during the first sputtering most of the residues were removed. The intensity of the first component at 1116 eV increases upon increasing of the sputtering time and can be attributed to metallic gallium [26]. The second contribution is due to the oxide layer (Ga_2O_3 [26]) formed upon exposure to air. It was not possible to remove the oxide film entirely, because of the supposable oxide film thickness of more than 2 nm. This behavior has also been found for the electrodeposition of aluminium and silicon films in the ionic liquid $[Py_{1,4}]$TFSA [28].

3.3. *In situ* STM measurements

In order to get more insight in the electrodeposition process the electrochemical behavior of Au(1 1 1) was investigated in an extremely pure ionic liquid $[Py_{1,4}]$TFSA and in its mixture with 0.5 mol L^{-1} $GaCl_3$ by *in situ* scanning tunneling microscopy (STM). Between OCP (−0.2 V *vs.* Pt) and −1.0 V gold shows a defect rich surface pattern typical for the Au(1 1 1) structure in extremely pure $[Py_{1,4}]$TFSA (Fig. 6a). The defects are one monolayer deep and the step heights between the terraces can be identified to be 250 ± 30 pm. The width of the defects is between 10 nm and 20 nm (Fig. 6a, height profile 1). This is quite a typical surface behavior of Au(1 1 1) in $[Py_{1,4}]$TFSA [29]. Although this structure of the Au(1 1 1) at OCP is quite reproducible we would like to mention that the exact structure can vary a bit from experiment to experiment. By reducing the electrode potential the number and the depth of these defects decreases (Fig. 6b, height profile 2). At −2.0 V with the exception of few vacancies the typical terraces of Au(1 1 1) are probed (Fig. 6c).

The sequence of *in situ* STM images in Fig. 7 represents the electrochemical behavior of Au(1 1 1) in 0.5 mol L^{-1} $GaCl_3$/$[Py_{1,4}]$TFSA. Fig. 7a represents an *in situ* STM image obtained after about 2 h of tip approaching. During this time the OCP (cell switched off) was observed to increase from −0.2 V *vs.* Pt to a limiting value of

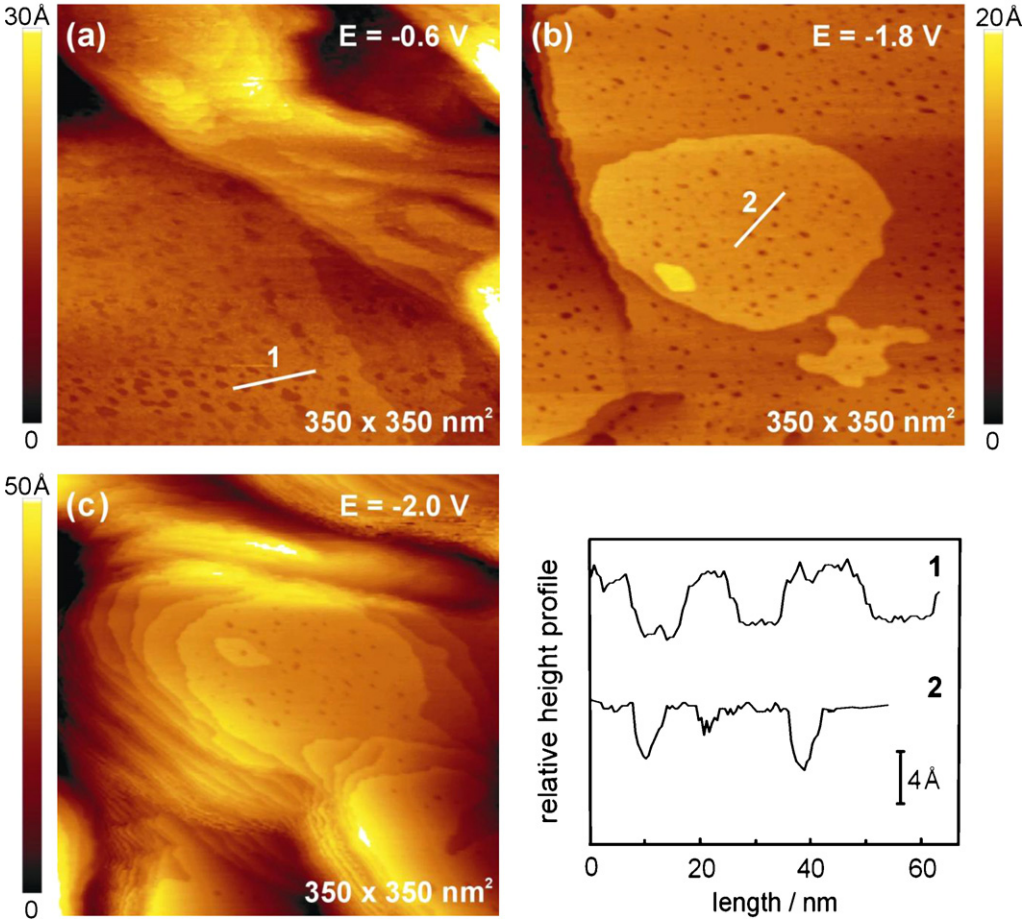

Fig. 6. *In situ* STM images of Au(1 1 1) in ultrapure $[Py_{1,4}]$TFSA ionic liquid. (a) Between OCP (−0.2 V *vs.* Pt) and −1.0 V gold shows a worm-like surface pattern typical for Au(1 1 1) structure in this ionic liquid. The width of the defects is between 10 nm and 20 nm (height profile 1). (b) By reducing the electrode potential the number and the depth of the defects decreases (height profile 2). (c) At −2.0 V with the exception of a few vacancies typical Au(1 1 1) terraces are probed.

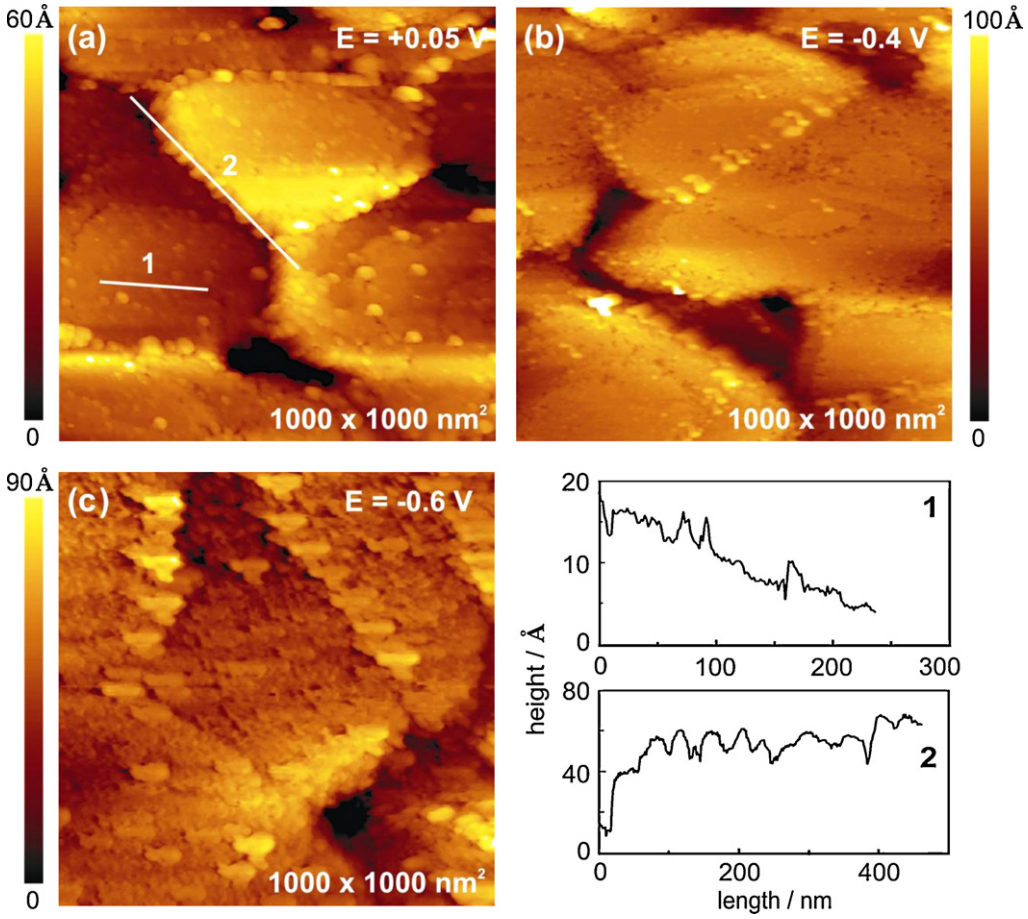

Fig. 7. The series of *in situ* STM images represents the electrochemical behavior of Au(1 1 1) in 0.5 mol L^{-1} $GaCl_3$/[$Py_{1,4}$]TFSA. The cell was switched off during the tip approach. With time the OCP increased from −0.2 V until the limit of +0.05 V. (a) There is a deposit on the surface made up of very small islands of 10–30 nm in width and heights in the nanometer regime (height profile 1). The step edges are decorated with the bigger crystals of the deposit (height profile 2). (b) When the electrode potential is decreased the crystals start to grow. (c) At −0.6 V the surface is slowly covered by a thin layer of the deposit.

0.05 V *vs.* Pt. The Au(1 1 1) surface can hardly be identified. Obviously there is already a deposit on the gold surface that seems to be made up of very small islands of 10–30 nm in width and heights in the nanometer regime (Fig. 7a, height profile 1). The step edges are also decorated (Fig. 7a, height profile 2). There are no such islands at this electrode potential in the pure ionic liquid, as shown in Fig. 6. These observations reveal that an electroless deposition starts as soon as Au(1 1 1) gets in contact with the $GaCl_3$-containing electrolyte. Such an effect is well known from aqueous electrochemistry. Recently examples of electroless deposition have been reported in deep eutectic solvents [30] and in ionic liquids [31]. Abbott et al. [30] showed that electroless deposits of silver up to several microns on copper can be obtained from a choline chloride-based deep eutectic solvent. They found that during Ag deposition silver ions reach the copper substrate and copper ions diffuse to the bulk of the solution mainly through the pores and channels in the silver deposit. Electroless deposition of Au was observed on glassy carbon from H[$AuCl_4$] (0.015 M) in 1-butyl-3-methylimidazolium bis(trifluoromethylsulfonyl)amide, [BMIm]TFSA [31]. At the first glance it does not make sense at all that both from the (aqueous) potential scale and from the electrochemical window of the ionic liquid an electroless deposition of gallium occurs. We will present more results on gallium electroless deposition later in this paper.

Switching the cell on and reducing the potential the deposit starts to grow (Fig. 7b). At −0.6 V (potential regime of reduction process *A*) the surface gets – very slowly – more and more covered by a thin layer of a deposit (Fig. 7c). An *in situ* I/U tunneling spectrum of the deposit reveals a typical metallic behavior (Fig. 8). In our experience current/voltage tunneling spectra of metals in ionic liquids can be linear, before an exponential rise prevails at higher voltages. It is an open question to which extent the already mentioned solvation layers at the IL/metal interface influence tunneling spectra. If the electrode potential is further reduced a massive deposition sets in leading to a bad quality of the STM images. At such

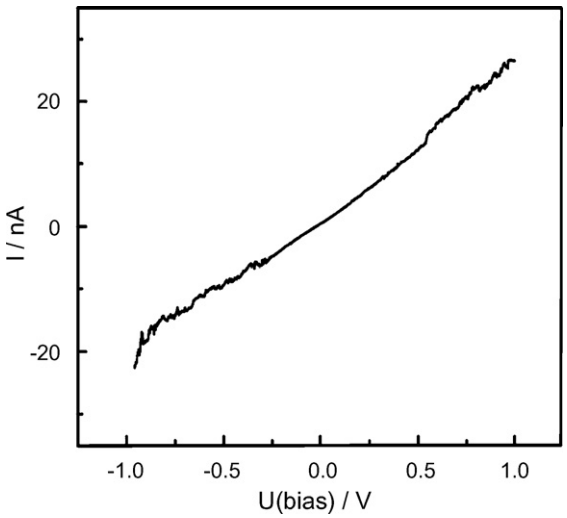

Fig. 8. *In situ* current/voltage tunneling spectrum of the electrodeposit obtained on Au(1 1 1) in 0.5 mol L^{-1} $GaCl_3$/[$Py_{1,4}$]TFSA exhibits metallic behavior.

negative electrode potentials no reasonable STM pictures can be obtained.

The behavior changes distinctly if the potential is kept constant at the initial potential (−0.2 V *vs*. Pt) during the tip approaching. In this case, as depicted in Fig. 9a, even at −0.2 V *vs*. Pt the gold surface is completely covered by a layer of the electrodeposit. The deposit consists of small islands of 50–100 nm in width and 2–5 nm in height (Fig. 9a, height profile). An *in situ* I/U tunneling spectrum of this deposit also exhibits typical metallic behavior. We did not observe any deposit up to −0.4 V *vs*. Pt when highly oriented pyrolytic graphite (HOPG) was used as a working electrode. The *in situ* STM image of HOPG in 0.5 mol L^{-1} $GaCl_3$/$[Py_{1,4}]$TFSA is presented in Fig. 9b for comparison purposes.

3.4. Gallium electroless deposition

It was found and described above that if the gold electrode is immersed in the solution of 0.5 mol L^{-1} $GaCl_3$ in $[Py_{1,4}]$TFSA ionic liquid at 24 °C, the initial OCP −0.2 V *vs*. Pt increases until the limited value of +0.05 V *vs*. Pt is achieved. In contrast, when HOPG is applied as a working electrode the OCP remains stable. In order to shed more light on this reaction we performed chemical experiments. When the gold substrate is directly immersed into the liquid, after about 1 h a very-thin gray layer is observed on the gold surface. On increasing the temperature to 36 °C, a shorter time is required for the deposit to be noticed. At 60 °C, only 10 min are necessary for the gold surface to be totally covered by quite a thick layer of gallium. Fig. 10 shows the photographs of the gold surface before (a) and after (b) an immersion experiment for 1 h in 0.5 mol L^{-1} $GaCl_3$/$[Py_{1,4}]$TFSA at 60 °C. As can be seen from the SEM micrograph in Fig. 10c, the morphology of the deposit presents a nodular structure and is rougher in comparison with Fig. 3a. An EDX analysis confirms without any doubt the deposit to be gallium. We should mention that, if platinum or glassy carbon substrates are employed for this study, no deposit is observed at any temperature in the range of 24–100 °C. As this was a pure chemical experiment, it is of interest what the anodic reaction is upon deposition of gallium. From our experience $[Py_{1,4}]$TFSA ionic liquid is quite stable under the applied conditions. In the following we shortly summarize that at least a cathodic instability of the TFSA ion is known. MacFarlane et al. [32] have reported that a cathodic breakdown of the $TFSA^-$ anion can occur. However, in our case the electroless deposition of gallium sets in at −0.2 V *vs*. Pt quasi-reference electrode. This electrode potential is almost 1.8 V more positive than the electrode potential required for the cathodic decomposition of the $TFSA^-$ anion. The irreversible reduction of the organic cation $[Py_{1,4}]^+$ sets in, as depicted in Fig. 1 (inset), at even more negative electrode potentials (−3.2 V *vs*. Pt). Thus, it is very unlikely that any of the breakdown products reduces $GaCl_3$ if the cathodic processes of the ionic liquid are that far away from the applied/measured electrode potential. From the electrochemical window it is unlikely as well that the ions of the liquid are oxidized by $GaCl_3$. Furthermore, in our experience, a decomposition of the $[Py_{1,4}]$TFSA is always accompanied by a change in the colour of the solution as well as by a typical amine ("fish-like") smell, which was definitely not observed during the electroless deposition experiments reported here. One could argue that Cl^- from $GaCl_3$ reduces Ga(III), but then there might be chlorine evolution which we also did not observe. Therefore a reasonable (though much surprising) assumption is that during gallium electroless deposition gold is oxidized, especially as there was definitely no gallium deposition when the experiment was done with platinum and glassy carbon under exactly the same conditions. Either gold (and not platinum or graphite) is under these conditions a catalyst for IL breakdown with the result that the breakdown products reduce $GaCl_3$ to Ga, or Au is the reducing agent itself. In chloroaluminate ionic liquids Cu^{2+} can oxidize Au to Au^+ [33], which is due to a totally different complexation in comparison to aqueous solutions. In chloroaluminates Cu^{2+} has a much more positive electrode potential than in water and in the presence of halide gold ions are stabilized as complexes making gold more reactive. Although a direct evidence is currently missing (and would require many more experiments on the solution/interface

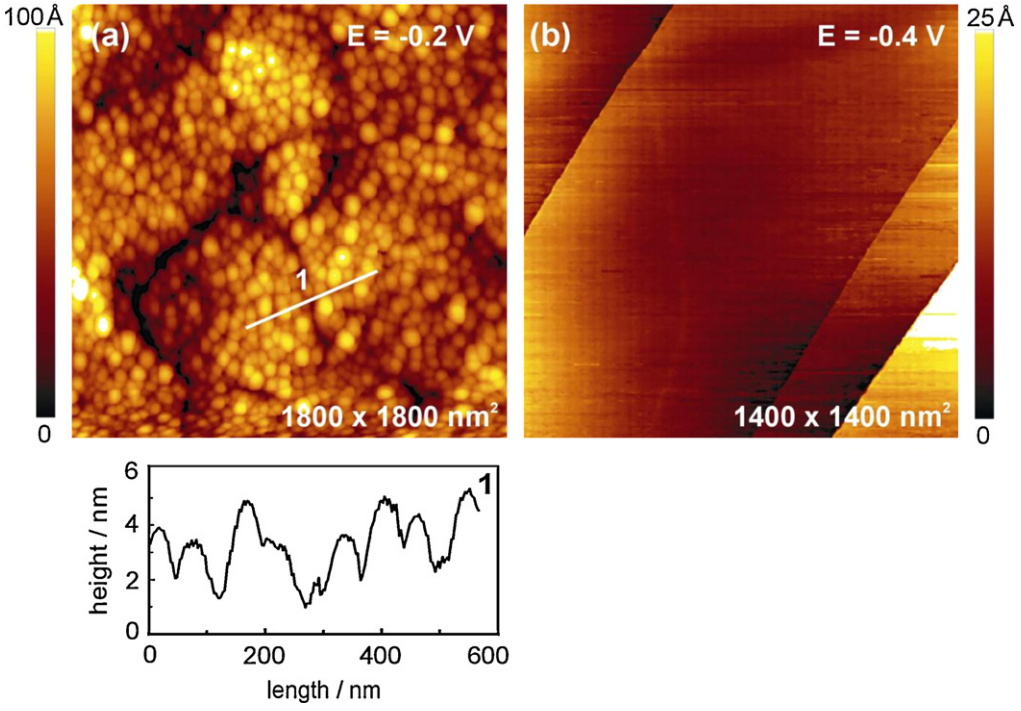

Fig. 9. *In situ* STM images of: (a) Au(1 1 1) in 0.5 mol L^{-1} $GaCl_3$/$[Py_{1,4}]$TFSA. The cell was switched on during the tip approaching. The surface is completely covered by quite a thick layer of the deposit, which consists of islands of 50–100 nm in width and 2–5 nm in height (height profile); (b) HOPG in 0.5 mol L^{-1} $GaCl_3$/$[Py_{1,4}]$TFSA. There is no deposit obtained on the surface under comparable conditions.

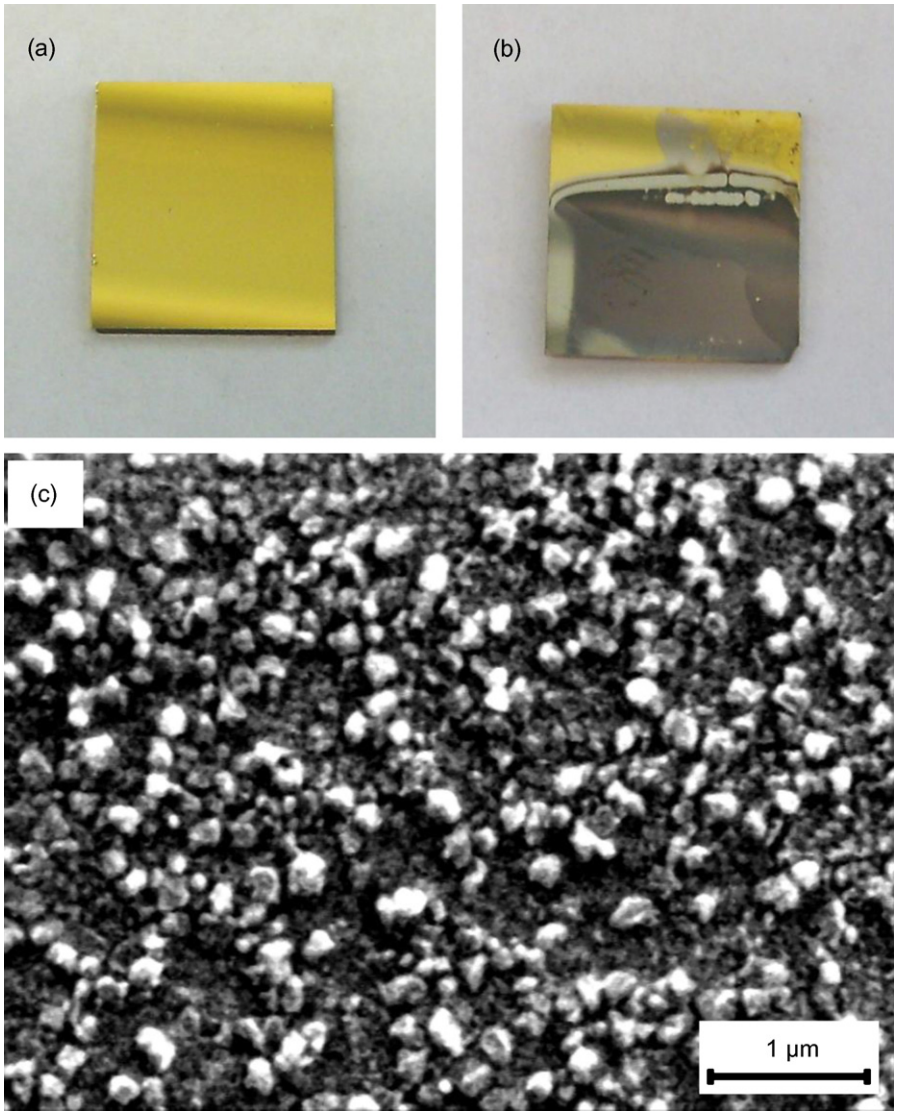

Fig. 10. The photographs of: (a) the clean gold electrode; (b) gold with the deposit after 1 h immersion at the OCP in 0.5 mol L^{-1} $GaCl_3$/[$Py_{1,4}$]TFSA at 60 °C. (c) SEM image of the deposit.

chemistry of Au/$GaCl_3$) it is not excluded that Au is the reducing agent for $GaCl_3$ here, too. This reaction might further be facilitated due to the presence of halide which is known to form complexes ($AuCl_4^-$) with gold. A final answer can – unfortunately – not be given at the moment and would require many more *ex situ* experiments with further ionic liquids as well as a detailed analysis of the solution.

The melting point of gallium is roughly 30 °C – close to room temperature – thus if an alloying of gallium with any metal occurs its low melting point will facilitate diffusion into the other metal. Based on the bulk phase diagram, the Au–Ga system contains at least two intermetallic compounds, AuGa and $AuGa_2$, even at room temperature. Hence in our experiment we have to expect a strong interaction between Au and the deposited Ga.

It is an experimental fact that if Au(1 1 1) is immersed in the electrolyte an electroless deposition of Ga occurs on the gold surface (Fig. 7a), but not on platinum or glassy carbon. Furthermore the deposition of Ga occurs both on the terraces and at the step edges of gold where the chemical potential is per se different. From the phase diagram it is likely that Ga atoms deposited on the gold diffuse first into the top most layer of the gold lattice, thus gradually saturating the gold surface. When the surface becomes saturated the first Ga islands form on the gold terraces. At the step edges Ga atoms can also diffuse into the gold lattice. From our experiments the Au–Ga alloy formed in the electroless potential regime prevents further Ga deposition finally stopping it (Fig. 7a). If the electrode potential is always kept at −0.2 V the deposition lasts until a complete layer of deposit covers the gold surface (Fig. 9a). With more negative electrode potentials finally a “normal” gallium deposition sets in.

4. Conclusions

Electrodeposition of Ga on Au(1 1 1) from 0.5 mol L^{-1} $GaCl_3$ in the air- and water-stable ionic liquid 1-butyl-1-methylpyrrolidinium bis(trifluoromethylsulfonyl)amide ([$Py_{1,4}$]TFSA) has been investigated by *in situ* scanning tunneling microscopy (STM), X-ray photoelectron spectroscopy (XPS) and cyclic voltammetry (CV). We have shown that quite surprisingly Ga can be electroless deposited in the employed ionic liquid as well as electrochemically. The CV Exhibits two redox processes. The first cathodic process at −0.3 V *vs.* Pt (*A*) might be attributed to gallium deposition on the gallium layer generated during an electroless process at OCP, fol-

lowed by the further gallium deposition at *B* on the just-formed phase. The first process (*A*) is presumably correlated with the formation of a Au–Ga surface alloy. XPS of bulk layers exhibits gallium, carbon and fluorine due to some residues from the ionic liquid and some oxygen due to exposure to air. *In situ* STM images evidence that Ga is electroless deposited on the Au surface. When the initial OCP (−0.2 V) is kept constant the gold surface is completely covered by Ga. The deposit consists of small islands of 50–100 nm in width and 2–5 nm in height. If the electrode potential is reduced the deposit grows further. An *in situ* I/U tunneling spectrum of the deposit gives typical metallic behavior. The gallium electroless deposition was found to depend on the nature of the electrode. No Ga deposit was observed when glassy carbon or platinum was employed as electrodes. However Ga electroless deposition took place on gold. This suggests that the anodic reaction involves gold oxidation although the oxidation of the ionic liquid can currently not be excluded totally. Further experiments have to be carried out in order to elucidate the mechanism of the electroless deposition of gallium on Au(1 1 1).

Acknowledgements

L.H.S. Gasparotto thanks Coordenação de Aperfeiçoamento de Pessoal de Nível Superior (CAPES) and Fundação de Amparo à Pesquisa do Estado de São Paulo (FAPESP) for a scholarship.

References

[1] J.C. Bailar, H.J. Emeleus, R. Nyholm, A.F. Trotman-Dickenson, Comprehensive Inorganic Chemistry, vol. 1, Pergamon Press, Oxford, 1973.
[2] R.K. Pandey, S.N. Sahu, S. Chandra, Handbook of Semiconductor Electrodeposition, Marcel Dekker, NewYork, 1996.
[3] I.A. Sheka, I.S. Chaus, T.T. Mityoreva, The Chemistry of Gallium, Elsevier, Amsterdam, 1966.
[4] T.I. Popova, I.A. Bagotskaya, E.S. Moorhead, in: A.J. Bard (Ed.), Encyclopedia of Electrochemistry of the Elements, Marcel Dekker, New York, 1978, Ch. VIII-3.
[5] W.M. Saltman, N.H. Nachtrieb, J. Electrochem. Soc. 100 (1953) 126.
[6] D.O. Flamini, S.B. Saidman, J.B. Bessone, J. Appl. Electrochem. 37 (2007) 467.
[7] D.O. Flamini, S.B. Saidman, J.B. Bessone, Thin Solid Films 515 (2007) 7880.
[8] F. Endres, Z. Phys. Chem. 218 (2004) 255.
[9] F. Endres, S. Zein El Abedin, Phys. Chem. Chem. Phys. 8 (2006) 2101.
[10] F. Endres, A.P. Abbott, D.R. MacFarlane (Eds.), Electrodeposition from Ionic Liquids, Wiley-VCH Verlag GmbH & Co, KGaA, Weinheim, 2008.
[11] S.P. Wicelinski, R.J. Gale, in: M.-L. Saboungi, D.S. Newman, K. Johnson, D. Inman (Eds.), Fifth International Symposium on Molten Salts (PV 86-1), The Electrochemical Society Softbound Proceedings Series, Pennington, NJ, 1986.
[12] M.K. Carpenter, M.W. Verbrugge, J. Electrochem. Soc. 137 (1990) 123.
[13] M.W. Verbrugge, M.K. Carpenter, AIChE J. 36 (1990) 1097.
[14] P.-Y. Chen, Y.-F. Lin, I.-W. Sun, J. Electrochem. Soc. 146 (1999) 3290.
[15] V.V. Smolenskii, A.L. Bove, A.A. Khokhryakov, A.G. Osipenko, Radiochemistry 45 (2003) 449.
[16] N. Borisenko, S. Zein El Abedin, F. Endres, J. Phys. Chem. B 110 (2006) 6250.
[17] D.R. MacFarlane, P. Meakin, J. Sun, N. Amini, M. Forsyth, J. Phys. Chem. B 103 (1999) 4164.
[18] W.G. Petro, T. Kendelewicz, I. Lindau, W.E. Spicer, J. Phys. Rev. B 34 (1986) 7089.
[19] T. Yamanaka, S. Ino, Phys. Rev. Lett. 89 (2002) 196101.
[20] R. Atkin, S. Zein El Abedin, R. Hayes, L.H.S. Gasparotto, N. Borisenko, F. Endres, J. Phys. Chem. C 113 (2009) 13266.
[21] R. Hayes, S. Zein El Abedin, R. Atkin, J. Phys. Chem. B 113 (2009) 7049.
[22] R. Atkin, G.G. Warr, J. Phys. Chem. C 111 (2007) 5162.
[23] M. Mezger, H. Schröder, H. Reichert, S. Schramm, J.S. Okasinski, S. Schröder, V. Honkimäki, M. Deutsch, B.M. Ocko, J. Ralston, M. Rohwerder, M. Stratmann, H. Dosch, Science 322 (2008) 424.
[24] M.V. Fedorov, A.A. Kornyshev, Electrochim. Acta 53 (2008) 6835.
[25] W. Zhou, T. Iwahashi, S. Inoue, Y. Katayama, H. Matsumoto, Y. Ouchi, Electrochemical Interface Structure of Neat Ionic Liquids on Metal Electrode Studied by In Situ Sum Frequency Generation Spectroscopy, Poster COIL-3, Cairns, Australia, 2009.
[26] G. Schön, J. Electr. Spectrosc. Relat. Phenom. 2 (1973) 75.
[27] C.D. Wagner, W.M. Riggs (Eds.), Handbook of X-ray Photoelectron Spectroscopy, Perkin Elmer, 1979.
[28] F. Bebensee, N. Borissenko, M. Frerichs, O. Höfft, W. Maus-Friedrichs, S. Zein El Abedin, F. Endres, Z. Phys. Chem. 222 (2008) 671.
[29] F. Endres, S. Zein El Abedin, N. Borissenko, Z. Phys. Chem. 220 (2006) 1377.
[30] A.P. Abbott, S. Nandhra, S. Postlethwaite, E.L. Smith, K.S. Ryder, Phys. Chem. Chem. Phys. 9 (2007) 3735.
[31] L. Aldous, D.S. Silvester, W.R. Pitner, R.G. Compton, M.C. Lagunas, C. Hardacre, J. Phys. Chem. C 111 (2007) 8496.
[32] P.C. Howlett, E.I. Izgorodina, M. Forsyth, D.R. MacFarlane, Z. Phys. Chem. 220 (2006) 1483.
[33] F. Endres, A. Schweizer, Phys. Chem. Chem. Phys. 2 (2000) 5455.